Toluene Removal By A Sequential Adsorption-Thermal Catalytic Process On Ag/Hopcalite

Shilpa Sonar, Jean-Marc Giraudon, Jean-Francois Lamonier, R. Morent, N. de Geyter, Axel Löfberg

Chemistry Europe
European Chemical Societies Publishing

WILEY VCH

Excellence in Chemistry Research

Announcing our new flagship journal

- Gold Open Access
- Publishing charges waived
- Preprints welcome
- Edited by active scientists

Meet the Editors of *ChemistryEurope*

Luisa De Cola
Università degli Studi di Milano Statale, Italy

Ive Hermans
University of Wisconsin-Madison, USA

Ken Tanaka
Tokyo Institute of Technology, Japan

ChemCatChem

Research Article
doi.org/10.1002/cctc.202200926

Chemistry Europe
European Chemical Societies Publishing

www.chemcatchem.org

Special Collection

Toluene Removal By A Sequential Adsorption-Thermal Catalytic Process On Ag/Hopcalite

Shilpa Sonar,[a, b] Jean-Marc Giraudon,*[a] Jean-François Lamonier,[a] Rino Morent,[b] Nathalie De Geyter,[b] and Axel Löfberg[a]

Hopcalite supported Ag (wt.%: 0.5; 1; 2; 10)-containing materials were prepared by wet impregnation followed by calcination at 400 °C for adsorption-thermal catalytic oxidation of toluene. Based on breakthrough experiments, the duration of the adsorption step was set around 38 min to minimize toluene loss at the outlet of the reactor (< 3 mol% of the amount of toluene adsorbed) allowing to determine a dynamic useful adsorption capacity for toluene. Thermal oxidation was performed in a He:O_2 (75:25) gaseous mixture from 20 °C to 250 °C (90 min) to assess the catalytic properties of the bifunctional materials throughout on-line monitoring of unreacted toluene and CO_2 during the temperature programmed reaction. Hop-0.5 Ag exhibited the best performance with a CO_2 yield of 98.9 %. Excellent redox properties and minimization of thermal effects were invoked to enhance total oxidation of toluene. Additionally, these bifunctional materials showed good stability under cycling conditions.

Introduction

Volatile organic compounds (VOCs) are considered as hazardous air pollutants which have detrimental effects on human health and environment. These negative impacts have prompted many countries to strengthen air quality legislation to reduce VOC emissions. VOCs are emitted from different sources, such as outdoor sources (industrial processes and transportation) and indoor sources (household products). For gaseous effluents containing low VOC concentrations, catalytic oxidation which is an effective way for VOC abatement is no longer cost effective.[1,2] Recognizing this, advanced adsorption processes have been proposed as cost-effective alternatives to current VOC abatement technologies. These advanced processes use the concept of «storage-regeneration» cycling.[3] This sequential method implies two steps: (i) first, the VOC is adsorbed on a bi-functional material which acts as adsorbent followed by (ii) the regeneration of the material (acting as a catalyst) through VOC total oxidation into CO_2 and H_2O. This regeneration step can be carried out using thermal oxidation,[4] non-thermal plasma exposure[5] or oxidation by ozone.[6] When using this cyclic approach, the design of the dual-functional material which should possess balanced properties between storage and regeneration is crucial. The bi-functional materials used for the storage of VOCs should have high and selective VOC storage capacity but should also be easily regenerated without any release of the parent VOCs and without the generation of secondary pollutants.

In their search for a good combined adsorbent/catalyst dual-functional material controlling low concentrations of toluene, Baek *et al.* carried out adsorption-catalytic regeneration over different transition metal-loaded zeolites HY.[7] Among all metal-loaded HY samples, the Ag/HY catalyst showed the lowest conversion temperature for toluene oxidation. The authors concluded that silver oxide or partially oxidized metallic silver species onto the surface of the metallic silver phase act as active redox sites during the oxidation reaction. The successful elimination of toluene by an adsorption/combustion process in humid conditions was reported by Wang *et al.* using Ru/hierarchical HZSM-5 zeolites as adsorbent/catalyst.[8] The good performance of these bi-functional materials was attributed to their increased external surface and mesoporous volume, their shortened diffusion length and their enhanced low-temperature reducibility. Additionally, simultaneous adsorption and oxidation of toluene were also recently carried out over TiO_2/SiO_2 and ZrO_2/SiO_2 mixed-metal oxides (MMOs) with varying compositions taking advantage of the fact that titanium- and zirconia-based materials have an excellent affinity towards toluene during adsorption and reaction.[9] It was shown that Ti-based MMOs were more efficient than Zr-based materials by displaying a higher dynamic capacity and toluene conversion as a result of their higher surface area and pore volume, their surface defects, and the presence of hydroxyl groups.

Inspired by these results, we have already investigated, in a previous study, the efficiency of potential adsorbent/catalytic

[a] Dr. S. Sonar, Dr. J.-M. Giraudon, Dr. J.-F. Lamonier, Dr. A. Löfberg
Univ. Lille, CNRS, Centrale Lille, Univ. Artois, UMR 8181-UCCS-Unité de Catalyse et Chimie du Solide
F-59000 Lille (France)
E-mail: :
E-mail: jean-marc.giraudon@univ-lille.fr
[b] Dr. S. Sonar, Dr. R. Morent, Dr. N. De Geyter
Research Unit Plasma Technology (RUPT)
Department of Applied Physics
Faculty of Engineering and Architecture
Ghent University
9000 Ghent (Belgium)

Special Collection This publication is part of a Special Collection on "French Conference on Catalysis 2022". Please check the ChemCatChem homepage for more articles in the collection.

materials such as a calcined commercial Hopcalite (Hop (Purelyst-MD101), nanorod ceria and UiO-66-SO_3H for toluene abatement considering a single adsorption/thermal catalytic oxidation process.[10] The highest CO_2 yield was 92% using Hop, which was the result of the best possible compromise between textural and redox properties. In order to optimize the effectiveness of Hop, we propose to disperse Ag on Hopcalite. Indeed, it is well known that silver can react with the aromatic ring of toluene allowing π-complexation during its storage phase. Additionally, it has been shown that Ag-containing mixed $CuMnO_x$ catalysts can improve the activity of carbon monoxide oxidation, which is the last step of total oxidation of toluene.[11–14]

In this work, Ag-promoted calcined Hopcalite (Purelyst-MD101) materials are prepared by wet aqueous impregnation of $AgNO_3$ on Hop followed by a drying step at 100 °C and finally calcined in flowing air at 400 °C for 4 h. Adsorption-desorption/oxidation of gaseous toluene on these supported Ag materials are assessed by uncompleted breakthrough experiments (adsorption time around 38 min) followed by temperature programmed reactions (TPR-O_2) in a $He:O_2$ (75:25) gaseous mixture (regeneration process). The efficiency of the regeneration step is discussed in terms of catalytic properties of the materials and is compared to their catalytic performances in the total oxidation of toluene in air from light-off curves. Additionally, a study in cycling mode is performed over Hop-1 Ag and Hop to apprehend the stability of these new developed dual-functional materials. Finally, the adsorbent/catalyst performances of the silver-based materials are discussed in terms of Ag speciation and dispersion on the calcined Hopcalite.

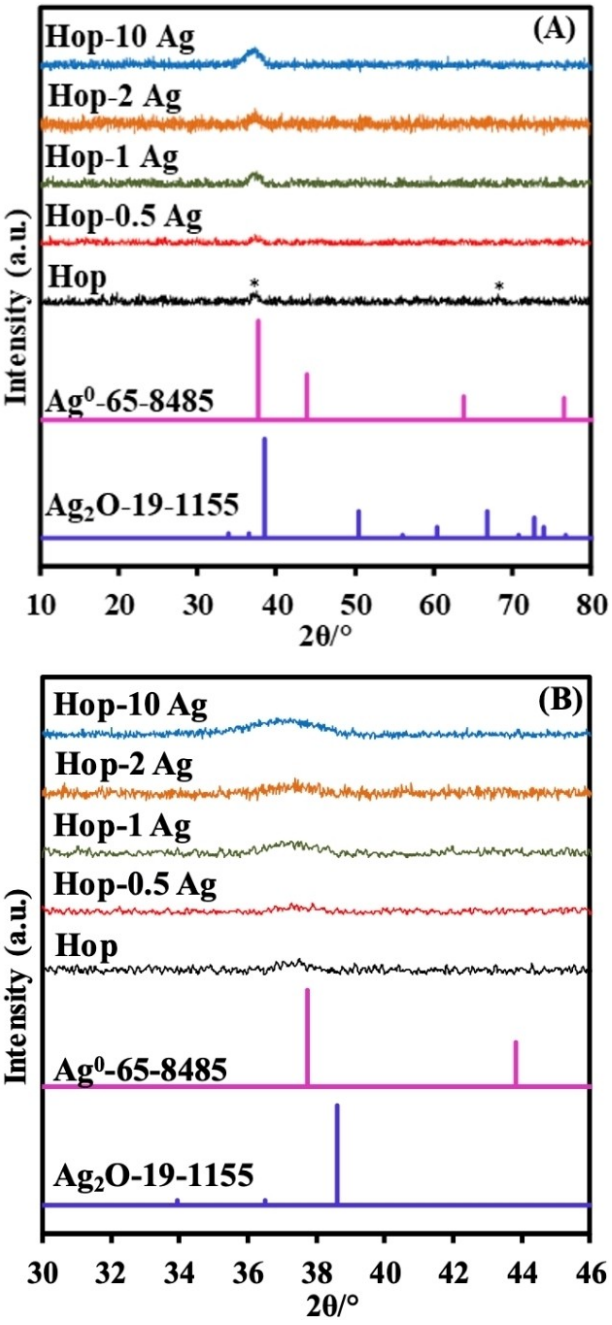

Figure 1. XRD patterns of (A) fresh Hop and silver-based Hop materials; (B) zoom in the 30°–46° 2θ range.

Results and Discussion

Catalyst Characterization

Structural and morphological characterization

The elemental bulk composition of Hop and as-prepared Hop-x Ag materials is given in Table 1. As expected, the Cu/Mn and K/Mn atomic ratios remain constant with increasing Ag loading. The X-ray diffraction (XRD) pattern (Figure 1A) of Hop shows two very low intensity peaks positioned at ~37° and ~66° which agrees with a highly disordered MnO_x.[15] When adding silver, we observe no diffraction peaks related to Ag (JCPDS-65-8485), Ag_2O (JCPDS-19-1155) or other silver-based oxides in the

Table 1. Physico-chemical properties of Hop and Hop-x Ag.

Material	Ag/Mn	Cu/Mn	K/Mn	S_{BET} [$m^2 g^{-1}$]	D_p[a] [nm]	V_p[b] [$cm^3 g^{-1}$]	T_{max}[c] [°C]	H_2 uptake [$mmol g^{-1}$]
Hop	–	0.28	0.078	232	7	0.45	341	11.07
Hop-0.5 Ag	0.006	0.27	0.074	118	11	0.40	314	11.12
Hop-1 Ag	0.008	0.29	0.078	118	14	0.40	311	10.93
Hop-2 Ag	0.025	0.27	0.072	115	14	0.40	307	11.20
Hop-10 Ag	0.105	0.28	0.074	175	8	0.40	307	11.23

[a] Maximum pore diameter, [b] Total pore volume, [c] H_2-TPR peak temperature.

2θ scan window 30°–46° (Figure 1B), not even for a silver content of 10 wt.%. These results indicate that Ag species are very well dispersed on Hop The transmission electron microscopy (TEM) images of Hop and Hop-x Ag samples (Figure 2) support these results as no Ag entities can be detected. All TEM images show the fringes of layer stacking with a lattice spacing of ~7.1 Å, which can be consistent with some disordered phyllomanganate material[16] along with the presence of amorphous areas.

Textural properties

The N_2 adsorption-desorption isotherms and pore size distribution of the materials are given in Figure 3 (A) and (B), respectively, and the corresponding textural properties are summarized in Table 1. The N_2 isotherm of Hop is of type IV with an H3 hysteresis loop indicating the presence of a mesoporous structure.[10] When adding Ag, it is observed that the shape of the original N_2 isotherm is preserved. However, the nitrogen uptake at P/P^0 below 0.05 is significantly reduced indicative of a partial loss of microporosity which is less pronounced for the Hop-10 Ag sample. As a consequence, after silver loading, a decrease of the specific surface areas is found with a concomitant rise of D_p from ~7 nm (Hop) to ~8–14 nm (Hop-x Ag) and a decrease of V_p from 0.45 to 0.40 $cm^3 g^{-1}$.

Redox properties

Figure 4 shows the H_2-TPR profiles of the samples. For Hop, the envelope is complex and shows 5 peaks in the temperature range 100–385 °C in line with the reduction of MnO_x into MnO and of Cu^{x+} into Cu(0). When adding silver, regardless of its content, it is found that the reduction process takes place in a smaller temperature range (100–345 °C) resulting from a downward temperature shift of the most intense H_2-consumption peak (see Table 1). A decrease of the number of peaks is also observed, from 5 to 3, except for Hop-10 Ag which shows an additional intense peak at 180 °C which can be consistent with the reduction of some Ag(I) species into Ag(0). Additionally, the peak around 150 °C shifted to lower temperature for Ag- (0.5–2 wt%) containing samples due to an increase amount of highly reduced species. It must be noted that the H_2 uptake for all samples under study shows very close values of 11.08 ± 0.15 mmol per gram of catalyst (see Table 1). As the contribution of the reduction of Hop is far greater than that coming from the reduction of Ag(I) species (detected using XPS, see below), it is not possible to discuss the silver distribution between Ag(I)/Ag(0). Based on these results, it can be however concluded that silver promotes the reduction of $CuMnO_x$ through spillover of hydrogen spillover.

Surface composition

XPS has been used to analyze the chemical states of elements and surface composition of these materials. Figure 5 and 6 depict the Ag 3d, Cu 2p, Mn 2p and Mn 3s XPS spectra of the Hop-based samples and XPS pertinent data are reported in Table 2. In any case, the Ag $3d_{5/2}$ photopeak is symmetric and centered at 367.6 ± 0.1 eV. This binding energy (BE) is consistent with that of Ag in Ag_2O[17–19] and lower than the BE for metallic silver which is located at 368.0 ± 0.2 eV,[20] thereby indicating the presence of Ag(I). The BE of Cu $2p_{3/2}$ at 933.0 ± 0.3 eV (Figure 6A) as well as the presence of satellite peaks ($I_{Cu2+satellite}/I_{Cu2p1/2} = 0.57 \pm 0.03$) confirm a chemical state of +2 for copper on all Hop samples.[21,22] It is also noteworthy that the BE of the

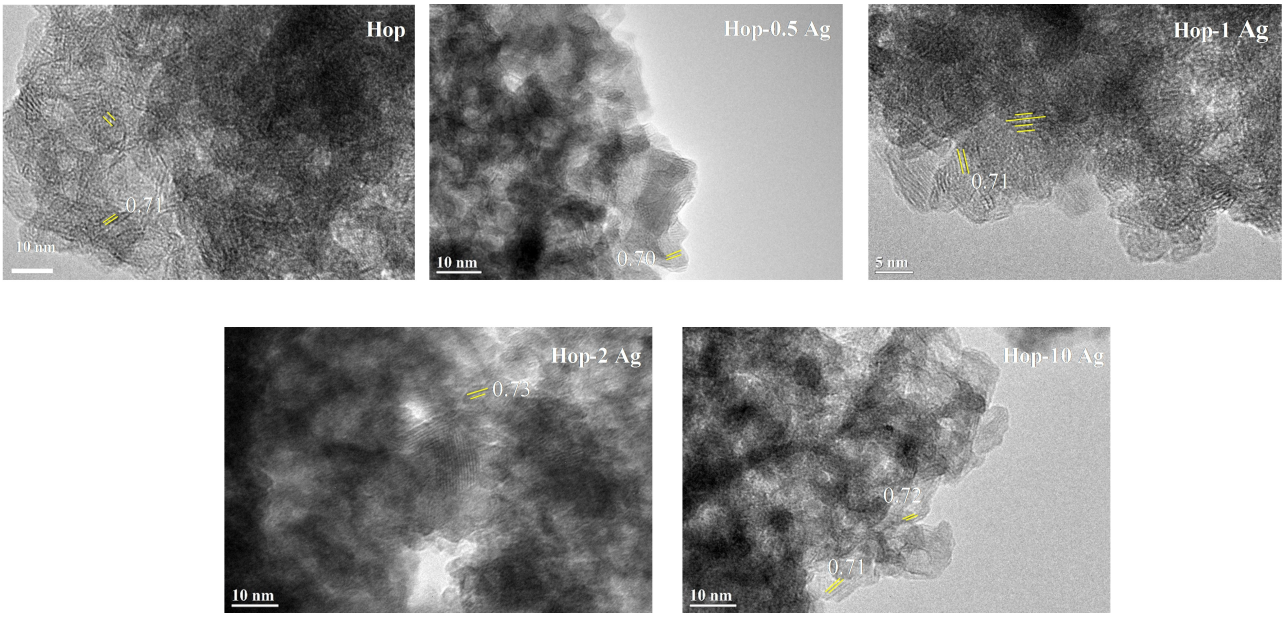

Figure 2. TEM images of Hop and silver-based Hop materials.

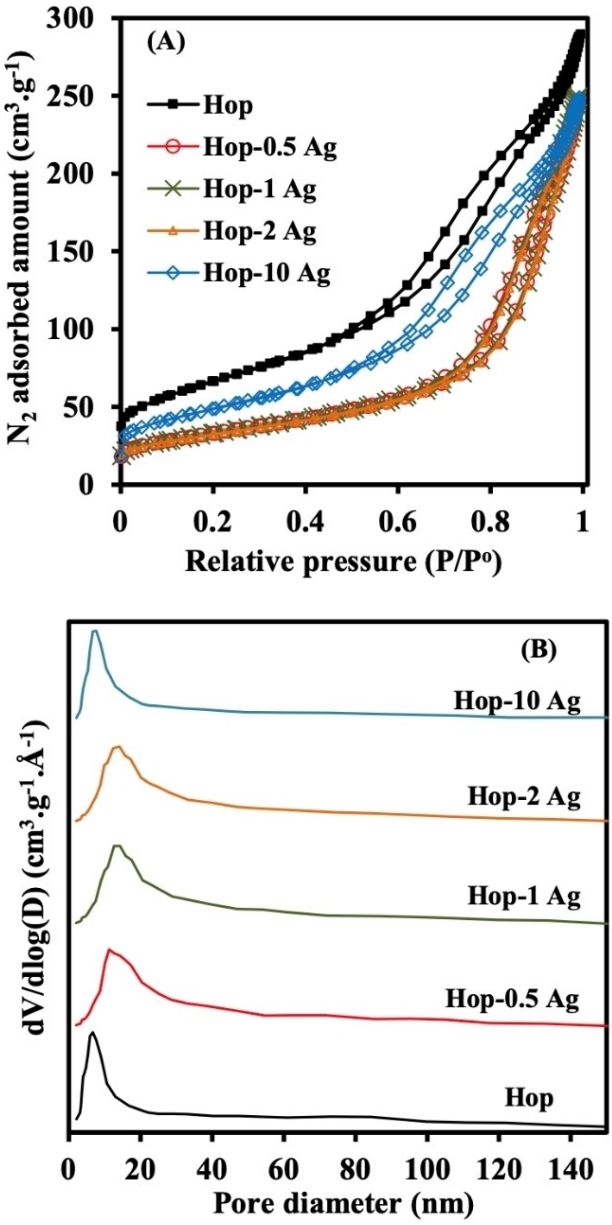

Figure 3. (A) N_2 adsorption-desorption isotherms and (B) pore size distribution of Hop and silver-based Hop materials.

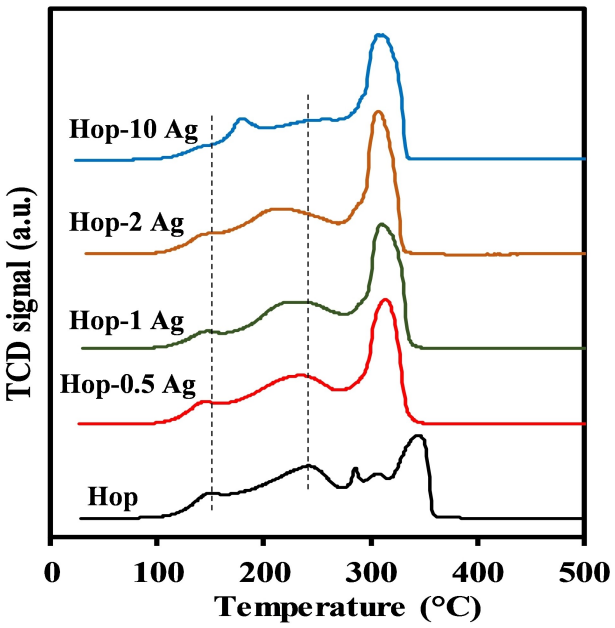

Figure 4. H_2-TPR profiles of Hop and silver-based Hop materials.

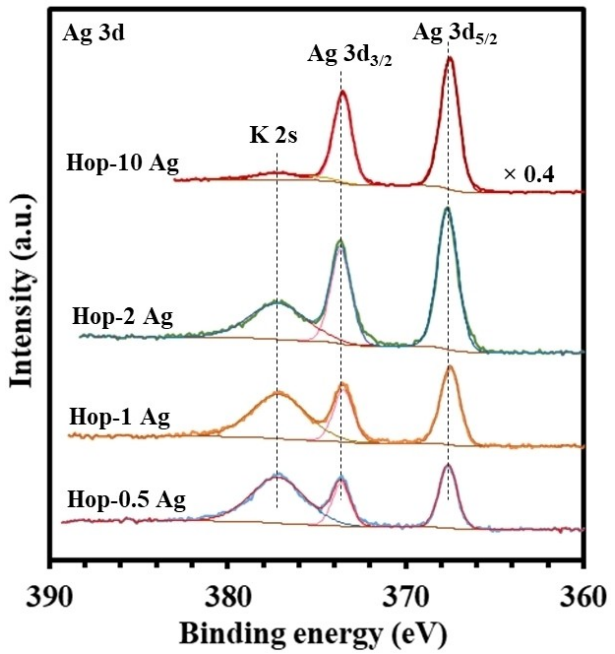

Figure 5. K 2s and Ag 3d core level spectra of fresh silver-based Hop materials.

electrons coming from the Mn $2p_{3/2}$ core-level at 642.0 ± 0.2 eV does not vary significantly with Ag content (Figure 6B). It has to be noted that the manganese average oxidation state (Mn AOS) obtained from the BE separation between the two components of the Mn 3s core level, as shown in Figure 6C,[23] is always slightly superior to 3.0 indicating the presence of Mn^{4+}/Mn^{3+} valence states as no Mn^{2+} component is detected on the Mn 2p spectra. This ratio clearly decreases with low amount of silver indicating more reduced Mn^{3+} formed on the surface. The asymmetrical O 1s photopeak of each sample (not shown here) has been decomposed in three components at BE of 529.7, 531.3 and 533.4 eV ascribed to surface lattice oxygen (O_{latt}), adsorbed oxygen (O_{ads}) and adsorbed molecular water species, respectively. It is found that the addition of Ag induces a significant increase of the O_{latt}/O_{ads} atomic ratio through the interaction between Ag and MnO_x. A plot of the Ag/Mn XPS ratio as a function of the Ag/Mn EDS atomic ratio presented in Figure 6D shows a silver enrichment for all catalysts which is more important for low Ag loadings in line with highly dispersed Ag(I) species at the surface of Hop. Furthermore, it should be noted that the Cu/Mn atomic ratio of 0.24 ± 0.02, the

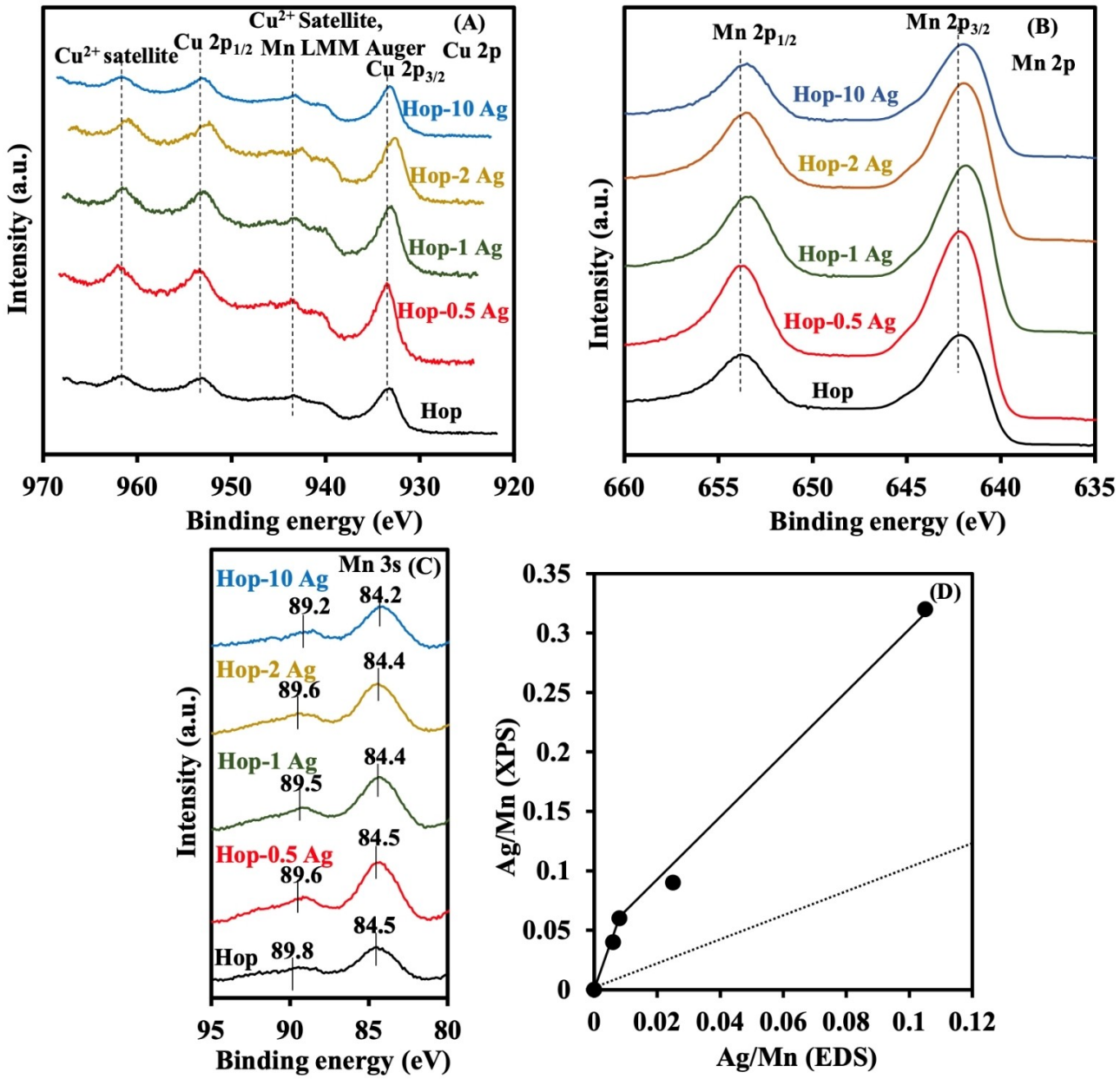

Figure 6. (A) Cu 2p, (B) Mn 2p, (C) Mn 3s core level XPS spectra of fresh Hop and silver-based Hop materials, (D) Ag/Mn (XPS) as a function of Ag/Mn (EDS).

Table 2. XPS peak positions of Ag $3d_{5/2}$, Mn $2p_{3/2}$, Cu $2p_{3/2}$, analysis data and atomic ratios for fresh Hop and Hop-x Ag samples, after one (S), three (3S) and five storage-regeneration sequences (5S).

Material	Peak Positions [eV]			Mn AOS	Atomic ratios					
	Ag $3d_{5/2}$	Cu $2p_{3/2}$	Mn $2p_{3/2}$		Ag/Mn	Ag/Cu	Cu/Mn	K/Mn	O/Mn	O_{ads}/O_{latt}
Hop	–	933.3	642.1	3.15	–	–	0.23	0.12	3.1	0.85
Hop-0.5 Ag	367.6	933.5	642.0	3.01	0.02	0.12	0.20	0.12	2.7	0.65
Hop-1 Ag	367.5	933.1	641.8	3.07	0.03	0.16	0.20	0.13	2.7	0.58
Hop-2 Ag	367.7	933.3	642.2	3.10	0.05	0.23	0.20	0.11	2.7	0.60
Hop-10 Ag	367.6	933.2	641.8	3.30	0.16	0.78	0.21	0.14	3.0	0.64
Hop-S	–	933.3	642.1	3.10	–	–	0.24	0.13	3.4	0.45
Hop-0.5 Ag-S	367.6	933.4	642.1	3.20	0.02	0.09	0.25	0.14	2.7	0.47
Hop-1 Ag-S	367.8	933.3	642.0	3.20	0.03	0.15	0.23	0.13	2.6	0.44
Hop-2 Ag-S	367.7	933.6	642.0	3.10	0.04	0.18	0.24	0.13	2.7	0.45
Hop-10 Ag-S	367.5	933.3	642.0	3.38	0.15	0.62	0.25	0.17	3.0	0.37
Hop-3S	–	933.5	642.2	3.40	–	–	0.23	0.13	2.6	0.47
Hop-1 Ag-5S	367.6	933.3	642.1	3.25	0.03	0.13	0.26	0.14	2.6	0.43

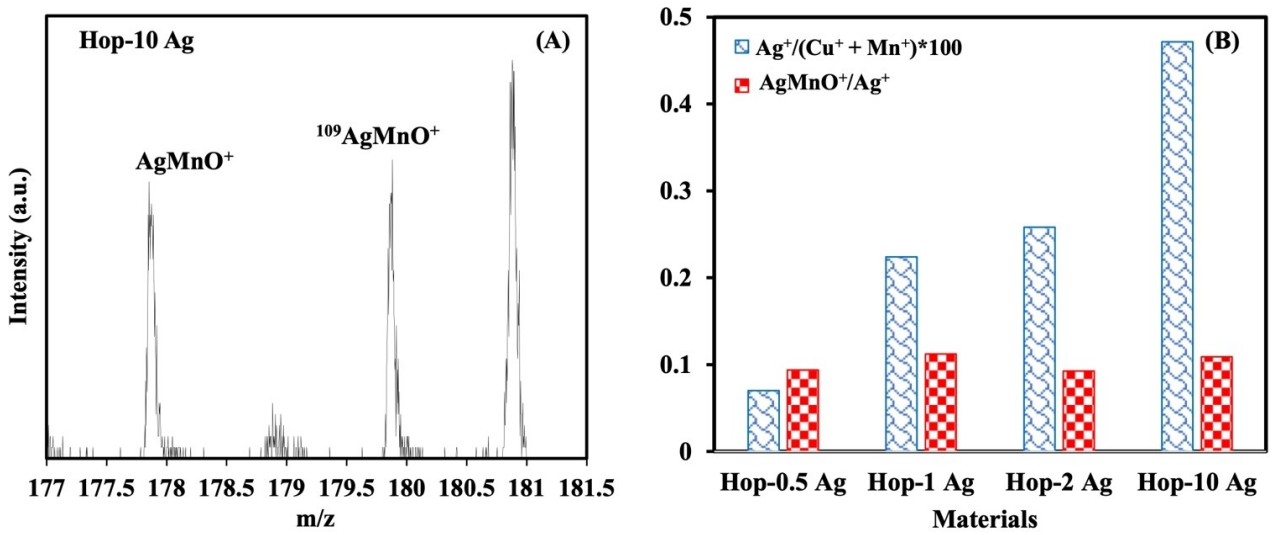

Figure 7. (A) ToF-SIMS spectra of Hop-10 Ag in polarity (+): m/z: 177–181.5, (B) ToF-SIMS intensity $Ag^+/(Cu^+ + Mn^+)$ and $AgOMn^+/Ag^+$ ratios.

K/Mn ratio of 0.11 ± 0.06, the O/Mn ratio of 2.8 ± 0.3 and the Na/Mn ratio of 0.03 ± 0.01 are not significantly affected by the presence of silver.

Static ToF-SIMS has been applied to survey the very outermost surface of the pure Hop and the Ag-based Hop catalysts taking advantage of the high surface sensibility of such spectroscopy. ToF-SIMS analysis reveals high concentrations of light elements such as K and Na on the surface for all samples. Moreover, NO_3^- is also observed as inorganic adsorbate. As expected, the ToF-SIMS (+) spectrum of calcined Hop exhibits a $CuOMn^+$ secondary ion which is also observed for the Ag-based samples.[21] Additionally, it is also detected the presence of $AgOMn^+$ secondary ions for all Ag-based catalysts as shown as an example on the ToF-SIMS (+) spectrum of the Hop-10 Ag sample in the m/z 177.0–181.5 range (Figure 7A). The detection of this last secondary ion supports the intimate interaction between Ag and Mn. In contrast, the $AgOCu^+$ secondary ion has never been detected. In order to assess the relative surface density of these new Ag-O–Mn interactions, the values of the ToF-SIMS intensity $Ag^+/(Cu^+ + Mn^+)$ and $AgOMn^+/Ag^+$ ratios estimated for a semi-quantitative analysis have been reported in Figure 7B. Based on these data, it is found a relative increase of Ag-O–Mn entities for the Hop-1 Ag sample as compared to the others. Such a result is important as an intimate interaction between Ag and Mn has been previously invoked in the enhancement of activity of MnO_x for total oxidation of toluene.[17,23]

To sum up, it was observed that Ag/Hopcalite bifunctional materials prepared via a wet impregnation route suffered from a partial loss of the specific area of Hopcalite probably due to the mode of Ag impregnation. Anyway, the beneficial effect of adding small amounts of silver Ag was observed throughout a better reduction of $CuMnO_x$ at low temperature due to hydrogen spillover. This could be explained by a better interaction between silver and manganese which was clearly evidenced through the increase of Ag–O–Mn interactions at the outermost layers of the materials. These interactions highlighted the presence of a possible mixed silver-manganese phase. On purpose, detection of a mixed silver manganese phase was previously reported to be highly reactive in the catalytic oxidation of toluene.[24]

Light-off curves of Hop and Ag-based Hop catalysts

Catalytic performances of Ag-based catalysts have been assessed for toluene total oxidation reaction in flowing air and compared to those of Hop taken as a reference. Toluene conversion into CO_2 as a function of temperature is given in Figure 8 and the relevant temperatures $T_x(CO_2)$ values (x = 10; 50; 90); temperatures at which 10, 50, and 90% of toluene is converted into CO2, are given in Table 3. The $T_{90}(CO_2)$ values are substantially lower for all Ag-containing samples as compared to Hop, while only the Hop-1 Ag sample outperforms Hop in terms of $T_{50}(CO_2)$ and $T_{10}(CO_2)$ exhibiting temperatures of 156 °C and 148 °C as compared to 185 °C and 157 °C for Hop. The catalytic properties (T_{50}) of various Ag-based MnO_x and $CuMnO_x$ obtained in the total oxidation of toluene (at similar concentration) are listed in Table 3. Clearly, this literature survey emphasizes the outstanding catalytic activity of Hop-1 Ag. Generally, MnO_2, preferentially δ-MnO_2[22,23] and α-MnO_2,[17,25,28] Mn_2O_3[26] and more rarely $CuMnO_x$[27] are the most effective systems for silver doping. The beneficial effect of Ag is usually attributed to highly dispersed Ag species and the formation of Ag–O–Mn bonds allowing the generation of more active oxygen through the existence of a Ag/MnO_2 interface.[17,23] The morphology of MnO_2 also influences the activity of the catalyst; in that way Ag supported α-MnO_2 nanowires allowing the formation of highly dispersed hemispherical Ag particles in strong interaction with the support are more efficient than nanorods and nanotubes.[25] It has also been reported that a low amount of well dispersed Ag on Mn_2O_3 nanowires showed

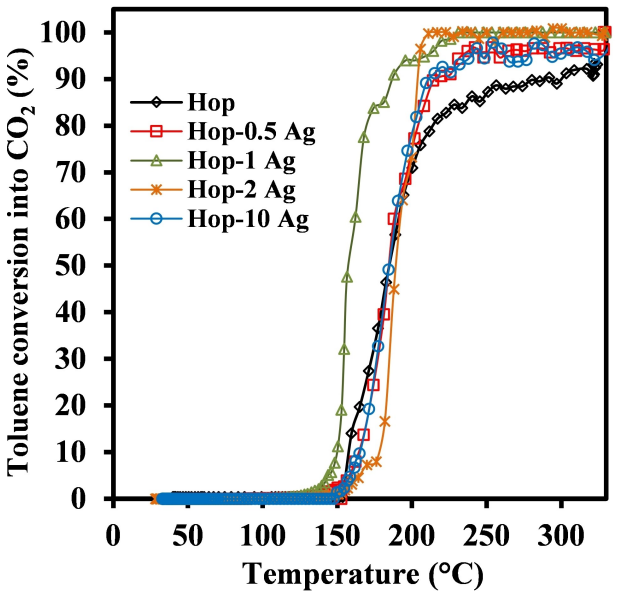

Figure 8. Toluene conversion into CO_2 as a function of temperature; inlet toluene concentration: 1000 ppm, gas hourly space velocity (GHSV) = 30,000 mL h^{-1} g^{-1}, temp: 330 °C to 150 °C (rate: −0.5 °C min^{-1}) to 25 °C (rate: −0.2 °C.min^{-1}).

good activity for toluene conversion.[26] Despite a decrease in specific surface area, silver doping in Hop-1 Ag can result in highly dispersed Ag(I) species on Hop leading to many Ag–O–Mn bridging bonds allowing much more active oxygen supply for the oxidation of toluene.[17,23,25]

Study of the adsorption/thermal oxidation sequence

To investigate the dynamic adsorption behavior of toluene over Hop and the Ag-containing materials, breakthrough curves were determined using an inlet toluene concentration of 100 ppm to ensure a significant duration of the unsaturated zone of the breakthrough curve as shown in Figure 9. Breakthrough times in the range of 38 min were observed for all samples, thereby leading to dynamic toluene adsorption capacities, ranging between 35.3 and 51.7 μmol g^{-1} (Table 4), depending on the Ag loading. Considering these results, the adsorption-thermal oxidation sequence was conducted in the following manner: a toluene adsorption step of about 38 min was first performed to minimize the toluene amount in the outlet (less than 3 mol% of the amount of toluene adsorbed). Then the samples were exposed to a He flow for 15 min to remove the reversibly adsorbed toluene followed by a temperature programmed desorption/reaction process from 20 °C up to 250 °C using a heating rate of 2 °C min^{-1}. Table 4 shows that the useful adsorption capacities (in μmol g^{-1}) modestly increase with increasing Ag loading: Hop (35.3) < Hop-0.5 Ag (35.8) < Hop-1 Ag (40.1) < Hop-2 Ag (40.5) < Hop-10 Ag (51.7). This can be attributed to the introduction of new Ag(I)-based active sites for toluene adsorption mitigated by a decrease of the specific surface area.

Figure 10 shows the evolution of the toluene and CO_2 concentrations as a function of time during TPR-O_2 which is conducted after the sample exposure to a He flow. The temperature profile during TPR-O_2 as a function of time is also shown in this figure for sake of clarity. Only the temporal

Table 3. Literature survey on Ag-based catalysts for toluene oxidation.

Material	Concentration [ppm]	GHSV [mL g^{-1} h^{-1}]	$T_{10\ CO2}$ [a] [°C]	$T_{50\ CO2}$ [b] [°C]	$T_{90\ CO2}$ [c] [°C]	Reference
Hop	1000	30000	157	185	291	Present work
Hop-0.5 Ag	1000	30000	165	185	214	
Hop-1 Ag	1000	30000	148	156	188	
Hop-2 Ag	1000	30000	176	188	200	
Hop-10 Ag	1000	30000	165	184	209	
1 % Ag/MnO_2	1000	20000	150	210	210	[17]
1 Ag-δ-MnO_2	1000	60000	173	185	198	[25]
0.5 Ag-SDC-13 (δ-MnO_2)	1000	30000	220	230	245	[26]
Ag/MnO_2 wires	1000	20000	–	196	212	[27]
0.13 Ag/Mn_2O_3-ms	1000	40000	110	185	215	[28]
0.13 Ag/Mn_2O_3-imp	1000	40000	120	210	230	
0.5 Ag-MnCu	1000	30000	220	245	270	[29]
R–Ag/MnO_2	1000	10000	–	190	275	[30]

[a] T_{10}, [b] T_{50}, [c] T_{90}.

Table 4. Amount of toluene adsorbed ($qTol_{ads}$), toluene desorbed at room temperature ($qTol_{desRT}$) and temperature programmed reaction ($qTol_{desTPR}$), CO_2 formation (qCO_2) and yield of CO_2 (Y_{CO2}) for Hop and Hop-x Ag samples during toluene (100 ppm) adsorption followed by TPR-O_2 (He:O_2 = 75:25).

Material	$qTol_{ads}$ [μmol g^{-1}]	$qTol_{desRT}$ [μmol g^{-1}]	$qTol_{desTPR}$ [μmol g^{-1}]	T_{max} CO_2 [°C]	qCO_2 [μmol g^{-1}]	Y_{CO2} [%]
Hop	35.3	0.1	0.8	200	241.0	97.5
Hop-0.5 Ag	35.8	0.2	0.2	140	247.9	98.9
Hop-1 Ag	40.1	1.0	11.4	195	193.9	69.1
Hop-2 Ag	40.5	0.9	10.7	180	202.0	71.2
Hop-10 Ag	51.7	1.3	1.8	190	340.5	94.1

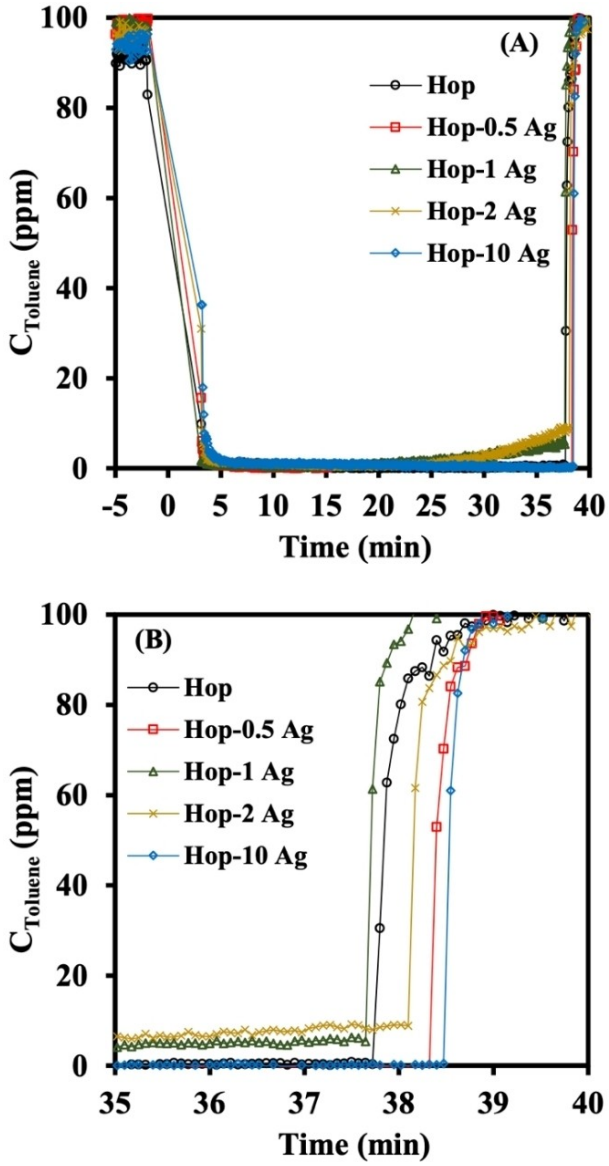

Figure 9. Concentration of toluene (in ppm) at the outlet of the reactor as a function of time during the toluene adsorption step over Hop, Hop-0.5 Ag, Hop-1 Ag, Hop-2 Ag and Hop-10 Ag (A) and zoom of the adsorption curve in the timeframe of 35 to 40 min (B).

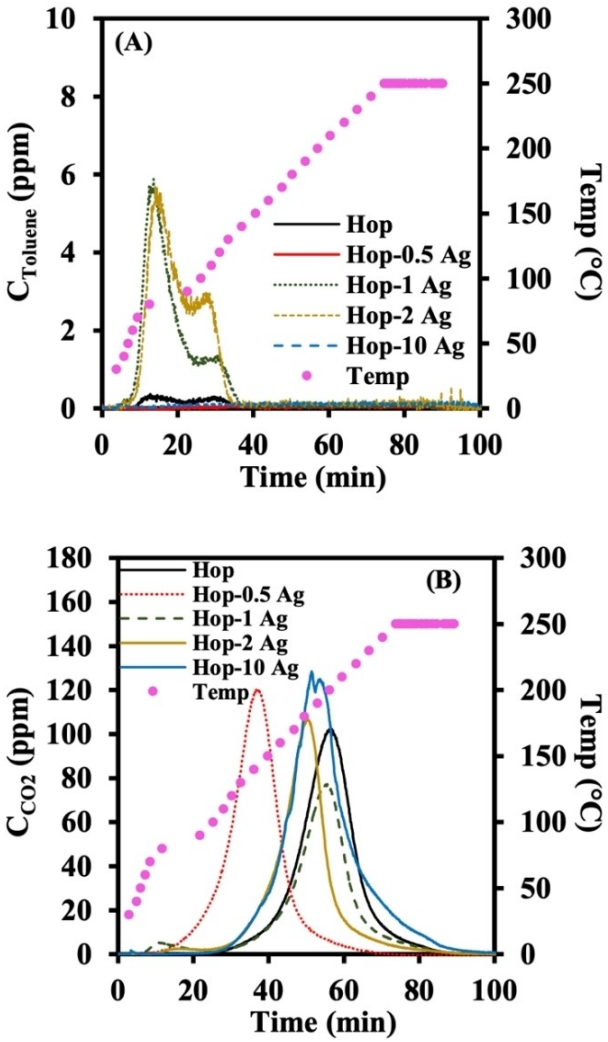

Figure 10. Evolution of the toluene (A) and CO_2 (B) concentration as a function of time during TPR-O_2 in an He : O_2 (75 : 25) atmosphere on Hop and silver-based Hop materials.

evolutions of these two species are shown in this study as these are the only detected gaseous products in the outlet. Figure 10 (A) and Table 4 clearly show that the amount of desorbed toluene during the TPR-O_2 process is very small (less than 1 μmol g^{-1}) on Hop and Hop-0.5 Ag. However, in the case of

Table 5. Amount of toluene adsorbed ($qTol_{ads}$), toluene desorbed at room temperature ($qTol_{desRT}$) and temperature programmed reaction ($qTol_{desTPR}$), CO_2 formation (qCO_2) and yield of CO_2 (Y_{CO2}) for cycling of fresh calcined Hop and calcined Hop-x Ag samples during toluene (100 ppm) adsorption followed by TPR-O_2 (He : O_2 = 75 : 25).

Material	$qTol_{ads}$ [μmol g^{-1}]	$qTol_{desRT}$ [μmol g^{-1}]	$qTol_{desTPR}$ [μmol g^{-1}]	qCO_2 [μmol g^{-1}]	Y_{CO2} [%]
Hop-1S	44.4	0.20	5.8	269.0	86.5
Hop-2S	42.4	0.15	6.3	251.6	84.7
Hop-3S	43.1	0.20	6.6	253.9	84.1
Hop-1 Ag-1S	40.1	1.0	11.4	193.9	69.1
Hop-1 Ag-2S	43.6	1.2	14.1	198.1	64.9
Hop-1 Ag-3S	37.4	1.3	8.5	193.3	73.8
Hop-1 Ag-4S	46.9	0.9	16.2	208.8	63.6
Hop-1 Ag-5S	35.4	1.0	8.0	184.7	74.5

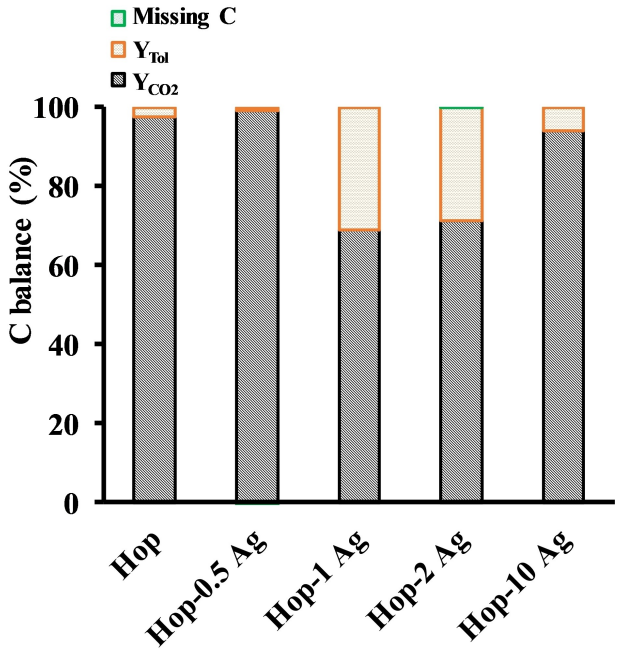

Figure 11. Carbon balance of calcined Hop and silver-based calcined Hop materials for one storage-regeneration sequence.

higher Ag loading, up to 2 wt.%, large quantities of toluene desorb through the detection of one large peak followed by a smaller second peak (approximately 10–11 $\mu mol\,g^{-1}$). The presence of the two peaks could possibly be due to an irregularity in the temperature profile, as already stated before.[10] For the Hop sample with an Ag loading of 10 wt.%, the desorption of toluene is again very low (Figure 10 (A)), reaching a value of 1.8 $\mu mol\,g^{-1}$ (Table 4). At a certain time, CO_2 appears in the outlet for all samples under study, which is due to the reaction between irreversibly adsorbed toluene and activated oxygen of the materials. As shown in Figure 10 (B), the CO_2 evolution appears as a single peak for all Hop samples, except for the Hop-1 Ag and Hop-2 samples, for which an additional small CO_2 peak at a very low temperature (T_{max} ~ 100 °C) is found. It is also noteworthy that the temperature of the major CO_2 peak decreases when adding Ag, with the largest downward shift of 60 °C being observed for Hop-0.5 Ag (Figure 10 (B) and Table 4). Additionally, for this latter sample, in contrast to the other samples, the CO_2 production ends before reaching 250 °C, which is the maximum temperature set for the thermal oxidation process. Comparing Figure 10 (A) with Figure 10 (B), it becomes evident that the pronounced desorption of unreacted toluene during TPR-O_2, which takes place for Hop-x Ag (x = 1; 2), occurs in the same timeframe as when the very small production of CO_2 is detected at low temperature. A possible explanation could be that these samples contain some highly active Ag related sites enabling the conversion of some toluene at very low temperature (below 100 °C). The heat generated by this latter exothermic process could provoke the unusual toluene desorption phenomenon observed for the Hop-1 Ag and Hop-2 Ag samples. As the toluene desorption largely disappears for the Hop-10 Ag sample, it is anticipated that these highly active Ag sites are no longer present on this particular sample. For each of the Hop samples under study, the amount of produced CO_2 and the corresponding CO_2 yield has also been determined and the results are summarized in Table 4. The CO_2 yields are the lowest for the samples Hop-x Ag (x = 1; 2). All other Hop samples show CO_2 yields above 94%, but the best CO_2 yield of 98.9% is obtained for the Hop-0.5 Ag sample, which is slightly higher than the CO_2 yield (97.5%) for Hopcalite. The CO_2 yields obtained in this study are in good agreement with previously reported values for Hop amounting to a CO_2 yield of 92%.[10] The carbon balance evaluated by using equation (2) are close to 100% for all samples (Figure 11).

Study of the sequential adsorption-thermal oxidation process

The stability of Hop-1 Ag has been assessed and compared to that of the free Ag sample and Hop by performing five and three consecutive sequences, respectively. Figure 12 shows the evolution of the toluene and CO_2 concentration as a function of time during TPR-O_2 for Hop (a, a′ respectively) and Hop-1 Ag (b, b′ respectively) samples throughout the different sequences under study. In addition, Table 5 summarizes different parameters of the adsorption-regeneration process including the amount of adsorbed toluene, the amount of desorbed toluene during exposure to the He flow and during TPR-O_2, the amount of produced CO_2 and the CO_2 yield. Figure 12 clearly shows that the TPR-O_2 profiles of desorbed toluene and of CO_2 superimpose indicating that the materials keep their original high efficiency for toluene oxidation in a cycling sequential adsorption-thermal oxidation process. The amount of adsorbed toluene (Table 5) remains similar considering the margin of errors. In each sequence, the carbon balance is close to 100% for both samples (Figure 13). It should be noticed that the XPS composition and nature of the state of the main elements, in particular for Ag samples, do not change significantly after the process (Table 2).

Effect of silver

Among other things, the valence state of silver species and silver content are expected to play a major role in the performance of these dual-functional materials for toluene oxidation. Based on XPS results it is found a chemical state of +1 for silver. The better dispersion of Ag species on the surface of Hop can be found for Hop-x Ag samples (x = 0.5;1 wt%) which exhibit the higher surface Mn^{3+}/Mn^{4+} and O_{latt}/O_{ads} atomic ratios throughout the formation of Ag–O–Mn bond. When looking at the storage step, the expected beneficial effect of Ag on toluene adsorption was rather small as two opposite effects occur. First, the introduction of some new Ag^{+} actives sites which can undergo electrostatic interactions with the aromatic ring of toluene can positively affect toluene adsorption.[31] However, this beneficial effect was partially countered by the decrease in specific surface area which could

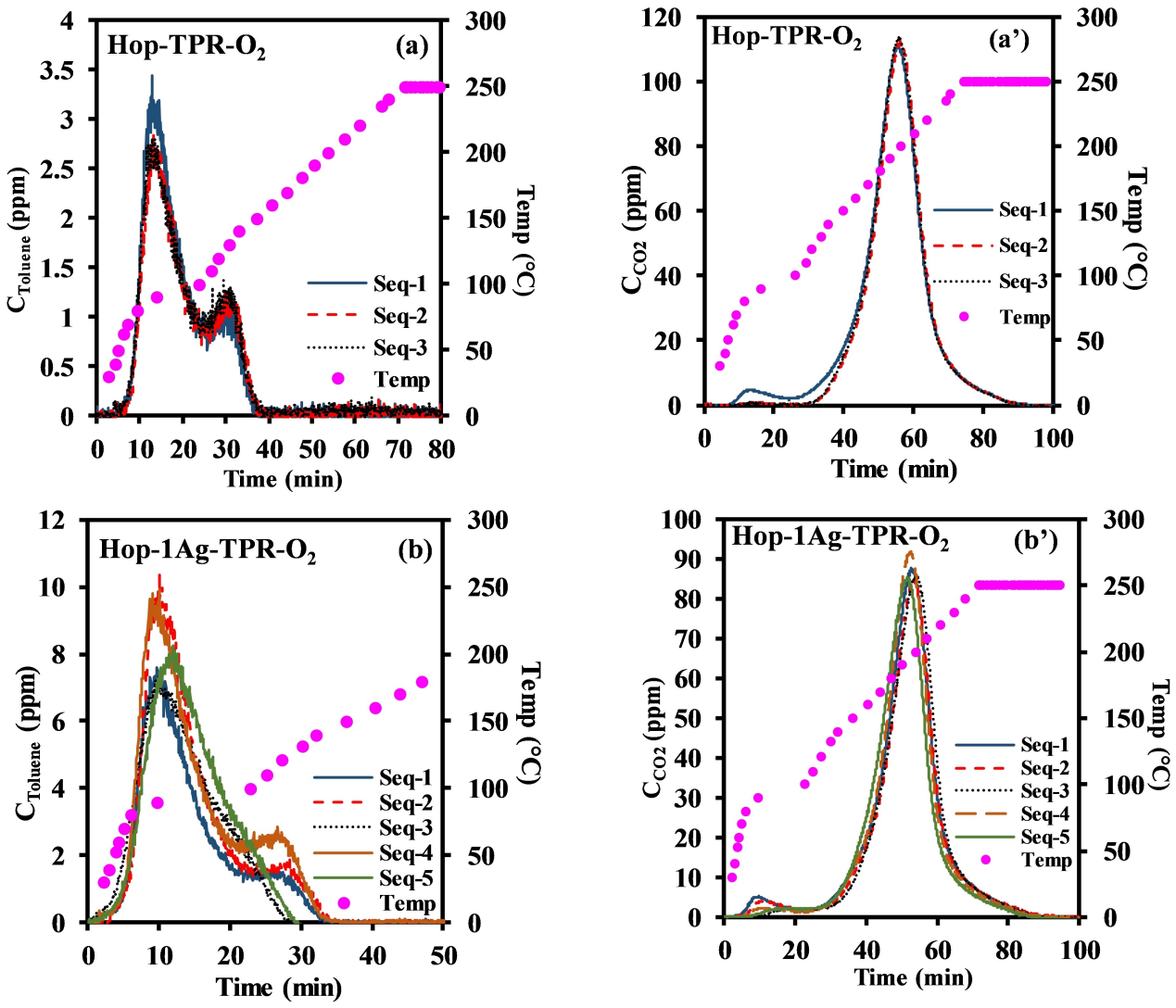

Figure 12. Evolution of the toluene (a, b) and CO_2 (a', b') concentration as a function of time during TPR in an oxidizing atmosphere over calcined Hop (a, a'), and calcined Hop-1 Ag (b, b').

be attributed to the negative impact of water on Hop. When considering the regeneration step, a higher CO_2 production is observed when loading a small amount of silver on Hopcalite (Hop-0.5 Ag) compared to pristine Hopcalite. However, in case of medium Ag loadings (Hop-1 Ag and Hop-2 Ag), the presence of some active sites provokes over-heating resulting in the unwanted desorption of unreacted toluene. This in turn has a negative impact on the overall efficiency of the process. Finally, it can be stated that Hop-0.5 Ag is the best suited bifunctional material for the storage-regeneration process as the CO_2 production occurs at the lowest temperature thereby guaranteeing a higher energy efficiency of the process. Considering that the oxidation of toluene may involve a Mars van Krevelen mechanism[32–34] implying lattice oxygen consumption to be replenish by air from the air stream, the beneficial of Ag addition to Hop consists in an increase of active lattice oxygen and a better reducibility of the catalysts. For low Ag/Mn ratios, the higher surface Mn^{3+}/Mn^{4+} and O_{latt}/O_{ads} atomic ratios resulting from the intimate interaction between Ag and Mn species lead to the formation of more reactive oxygen vacancies. As a result, the oxygen mobility and the oxygen activation are facilitate promoting the redox properties of Hop-0.5 Ag and Hop-1 Ag through the facile electron exchange between the different redox couples involving Mn, Cu and Ag and resulting in excellent reactivity.

Conclusion

Dual-functional adsorbent/catalyst materials consisting of silver doped calcined commercial Hopcalite Hop-x Ag (Ag wt% : 0.5; 1; 1; 2; 10) obtained via wet impregnation and calcined at 400 °C were assessed for total toluene oxidation using an adsorption-thermal catalytic process. It was shown that although the textural properties were not enhanced in the presence of Ag, the redox properties for low Ag/Mn ratios were

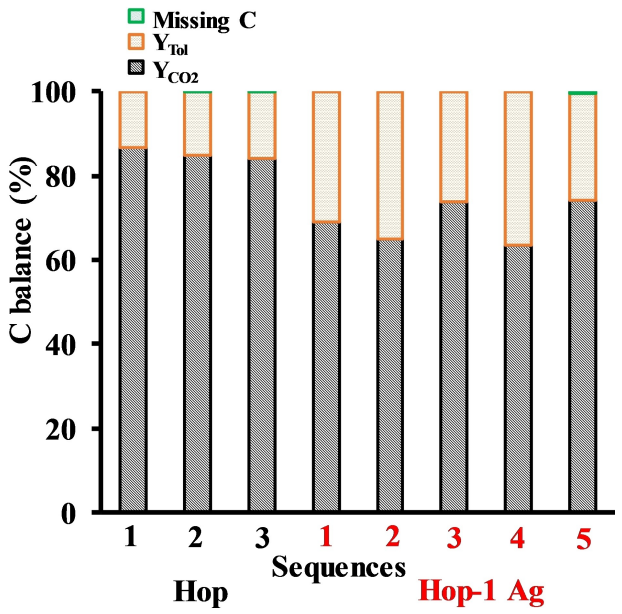

Figure 13. Carbon balance of calcined Hop and calcined Hop-1 Ag during the stability test.

in contrast improved due to homogeneous dispersion of Ag(I) species on Hopcalite throughout intimate interaction between Mn and Ag. As a consequence, the toluene adsorption capacities were very close for all dual-functional materials in the storage step as the introduction of possible new Ag(I) adsorption sites was counterbalanced by a partial loss of surface area. On the other hand, it was found that Hop-0.5 Ag was the best catalyst regarding the thermal catalytic-oxidation step because it combined enhanced redox properties and allowed minimization of thermal effects which decreased the efficiency of the process. Furthermore, the dual-functional adsorbent/catalyst materials showed good stability in cycling condition which was a key point in this advanced oxidation process.

Experimental Section

Catalyst preparation

All Ag-containing samples (Ag wt.%: 0.5, 1, 2, and 10) were prepared by wet impregnation over a calcined commercial Hopcalite (Purelyst MD-101; particle size: 200–300 μm, calcined at 300 °C for 4 h in flowing dry air; 2 °C.min^{-1}) labelled Hop. Typically, 100 mL of a silver nitrate solution ($AgNO_3$, 99.5%, Fluka) with expected amount of silver was added to ~1 g of Hop. The resulting suspension was stirred at 20 °C for 2 h at 300 rpm. The solvent was then removed under vacuum using a rotary evaporator (Büchi Rotavapor R-114; 60 °C; 20 rpm). The resulting samples were dried overnight at 100 °C and subsequently calcined in flowing dry air (0.2 L.min^{-1}) from 20 °C to 400 °C for 4 h (1 °C.min^{-1}). The catalysts were labeled Hop-x Ag, where x was the weight percentage of silver.

Catalyst characterization

The elemental composition (Ag, Cu, Mn and K) was determined using energy-dispersive X-ray spectroscopy (EDS, Hitachi S3400 N tungsten filament microscope, ThermoScientific). X-ray diffraction (XRD) patterns were recorded on a D8 Advanced Bruker AXS diffractometer equipped with a Cu $K_{\alpha 1}$ monochromatic radiation source ($\lambda = 1.5418$ Å at 40 kV/40 mA) and a Lynxeye super speed detector. The X-ray diffraction patterns were recorded within the range 10–80° with a 0.01° step size in 2θ and a step time of 1 s.

Transmission electron microscopy (TEM) characterization was performed using a TECNAI TEM which operated at 200 kV. The prepared powders were deposited onto a carbon-coated copper grid for TEM observation. N_2 physisorption isotherms were recorded at −196 °C using a TriStar II 3020 gas sorption analyzer from Micromeretics. Prior to the adsorption measurement, the catalysts were degassed at 150 °C for 5 h in a dynamic vacuum (P = 0.05 mbar). The Brunauer-Emmett-Telller (BET) method was used to calculate the specific surface area (S_{BET}). The Barret-Joyner-Halenda (BJH) equation was used to estimate the pore size distribution from the desorption branch. H_2-temperature programmed reduction (H_2-TPR) experiments were performed using a Micrometrics model autochem II 2920 equipped with a quartz U-shaped micro reactor. 50 mg of the samples was exposed to a 5% H_2/Ar gas mixture (50 mL min^{-1}) from 25 °C to 1000 °C at a heating rate of 10 °C min^{-1}. Time of flight secondary ion mass spectroscopy (ToF-SIMS) data were acquired using a ToF-$SIMS_5$ spectrometer (ION-TOF GmbH Germany) equipped with a bismuth liquid metal ion gun (LMIG). X-ray photoelectron spectroscopy (XPS) experiments were performed using an AXIS Ultra DLD Kratos spectrometer equipped with a monochromatic aluminum source (Al $K_\alpha = 1486.6$ eV), a hemispherical analyzer with constant △E/E and a charge compensation gun. The binding energies were referenced to adventitious C 1s at 284.8 eV. The Mn AOS was estimated by XPS from Mn AOS = 8.956–1.13 ΔE where ΔE was the binding energy separation between the doublet of Mn 3s peaks.[28] Elemental quantification and spectral decomposition were performed using CasaXPS® software. The Ag/Mn, Ag/Cu, Cu/Mn, K/Mn and O/Mn ratios were estimated from Ag $3d_{5/2}$, Mn $2p_{3/2}$, K $2p_{3/2}$, Cu $2p_{1/2}$ and O 1s core-levels.

Catalytic test process

Light-off curve study

The catalytic oxidation of toluene was carried out under atmospheric pressure in a continuous flow fixed bed pyrex-glass reactor with an inner diameter of 10 mm and a wall thickness of 1 mm. 0.2 g of catalyst was placed in the reactor for each run and the catalyst filled reactor was placed in an electrical furnace providing the required temperature for toluene oxidation. Before each experiment, the catalyst was pre-activated at 330 °C for 30 min (ramping rate 2 °C min^{-1}). The concentration of toluene was 1000 ppmv diluted in synthetic air, was stabilized at a flow rate of 100 mL min^{-1} (GHSV = 30000 mL h^{-1} g^{-1}). Catalyst performances were evaluated by decreasing the temperature from 330 to 150 (−0.5 °C min^{-1}) to 30 °C (ramping rate: −0.2 °C min^{-1}). The concentrations of the inlet and outlet gas stream were analyzed online by gas chromatography (R3000, SRA instrument) equipped with a thermal conductivity detector. The results were expressed in terms of toluene (C_7H_8) conversion X into carbon dioxide [CO_2, Eq. (1)]

$$X\ (\%) = \frac{[CO_2]_{out}}{7 \times [C_7H_8]_{in}} \times 100 \quad (1)$$

where X (%) was the conversion of toluene based on toluene oxidation and $[C_7H_8]_{in}$ and $[CO_2]_{out}$ were the species concentration measured at the inlet and outlet of the reactor, respectively.

The C balance was calculated from the sum of the toluene (Y_{Tol}) and CO_2 (Y_{CO2}) yields using Equation (2):

$$\text{C balance } (\%) = [Y_{Tol} + Y_{CO2}] \times 100 \quad (2)$$

Sequential adsorption-catalytic oxidation

The scheme of the home made experimental set-up for toluene abatement was previously given in literature.[10] Helium (He) was used as a carrier gas while toluene was provided from a premixed gas cylinder (0.1 vol% toluene in argon). The evolution of the gas phase composition was monitored using an online mass spectrometer (Omnistar, Pfeiffer Vacuum, Model GSD 301 02). Approximately 0.3 g of the sample was heated in flowing dry air (100 mL min^{-1}) at 150 °C for 4 h (5 °C min^{-1}) to clean the surface from absorbed species. The sample was then cooled down to 20 °C. Meanwhile, the required flow of He and toluene in argon was set to achieve the desired initial toluene concentration of 100 ppm. The toluene containing flow was passed through a by-pass and then switched to the reactor to perform the adsorption of toluene for 38 min. The amount of adsorbed toluene was calculated comparing the initial and residual toluene concentrations. The toluene/argon flow was then switched off and the helium flow adjusted to 100 mL min^{-1} to assess the amount of toluene reversibly adsorbed on the sample for 15 min. Finally, the sample was heated from 20 °C up to 250 °C (2 °C min^{-1}, hold at 250 °C for 1.5 h) in a He:O_2 (75:25) mixture. Simultaneously, the signals characteristic of toluene (m/z = 91), CO_2 (m/z = 44), possible by-products such as formic acid (m/z = 29), benzaldehyde (m/z = 77), and CO (m/z = 28) were recorded by the MS detector. The amount of toluene adsorbed denoted as the useful adsorption capacity ($q(Tol)_{ads}$), the amount of toluene desorbed at room temperature ($q(Tol)_{desRT}$) and desorbed during the temperature programmed reaction ($q(Tol)_{desTPR}$), the amount of CO_2 formation ($q(CO_2)_{TPR}$) and the CO_2 yield were calculated as follows [Eqs. (3)–(7)]:

$$q(Tol)_{desRT}\ (\mu mol.g^{-1}) = A \times \sum_{0}^{t} \left(\frac{P(Tol)_t + P(Tol)_{t+1}}{2} \right) \times \Delta t \quad (3)$$

$$q(Tol)_{desTPR}(\mu mol.g^{-1}) = A \times \sum_{0}^{t} \left(\frac{P(Tol)_t + P(Tol)_{t+1}}{2} \right) \times \Delta t \quad (4)$$

$$q(CO_2)_{TPR}\ (\mu mol.g^{-1}) = A \times \sum_{0}^{t} \left(\frac{P(CO_2)_t + P(CO_2)_{t+1}}{2} \right) \times \Delta t \quad (5)$$

$$q(Tol)_{ads}\ (\mu mol.g^{-1}) = q(Tol)_{desRT} + q(Tol)_{desTPR} + \frac{q(CO_2)_{TPR}}{7} \quad (6)$$

$$CO_2\ \text{Yield}\ (\%) = \frac{q(CO_2)_{TPR}}{7 \times q(Tol)_{ads}} \times 100 \quad (7)$$

where $P(Tol)_t$ and $P(CO_2)_t$ were the toluene and CO_2 partial pressures, respectively, at a given time expressed in atm, t was the time in min, $A = \frac{10^{-3}}{R \times T} \times \frac{F}{m}$ in which F was the total gas flow in mL min^{-1}, m was the weight of the material in g, T = 293 K and R = 8.0206 L atm mol^{-1} K^{-1}.

Stability tests in cycling sequential adsorption-catalytic oxidation

The sequential adsorption-catalytic oxidation was performed in a similar manner as explained before and was repeated over Hop and Hop-1 Ag for three (Hop-3S) and five times (Hop-1 Ag-5S), respectively. The suffix -xS (x = 1 to 5) was added to specify the number of already performed cycles. Between each sequence, the catalyst was kept under a static He:O_2 (75:25) atmosphere.

Acknowledgements

This research was supported by a European Program INTERREG V France-Wallonie-Flanders (FEDER) (DepollutAir). The Chevreul institute (FR 2638), the Ministère de l'Enseignement Supérieur et de la Recherche and Région Hauts-de-France are also acknowledged for supporting this work. This research was carried out in the French-Belgium associated international laboratory "Plasma & Catalysis" supported by the universities of Lille and Ghent. The authors also thank Nicolas Nuns, Maya Marinova, Pardis Simon, Laurence Burylo, Olivier Gardoll for their contribution to the ToF-SIMS, TEM, XPS, XRD, and H_2-TPR measurements, respectively.

Conflict of Interest

The authors declare no conflict of interest.

Data Availability Statement

Research data are not shared.

Keywords: Sequential adsorption-catalytic oxidation · Hopcalite · Silver · Toluene abatement

[1] Y. Guo, M. Wen, G. Li, T. An, *Appl. Catal. B* **2021**, *281*, 119447–119466.
[2] C. Yang, G. Miao, Y. Pi, Q. Xia, J. Wu, Z. Li, J. Xiao, *Chem. Eng. J.* **2019**, *370*, 1128–1153.
[3] B. Chen, L. Wu, B. Wu, Z. Wang, L. Yu, M. Crocker, A. Zhu, C. Shi, *ChemCatChem* **2019**, *11*, 3646–3661.
[4] C. Shi, B. Chen, X. Li, M. Crocker, Y. Wang, A. Zhu, *Chem. Eng. J.* **2012**, *200–202*, 729–737.
[5] S. K. P. Veerapandian, J. M. Giraudon, N. De Geyter, Y. Onyshchenko, C. Krishnaraj, S. Sonar, A. Löfberg, K. Leus, P. Van Der Voort, J. F. Lamonier, R. Morent, *J. Hazard. Mater.* **2021**, *402*, 123877–123889.
[6] Z. Ye, G. Wang, J. Giraudon, A. Nikiforov, J. Chen, L. Zhao, J. Wang, *J. Hazard. Mater.* **2022**, *424*, 127321–127330.
[7] S. W. Baek, J. R. Kim, S. K. Ihm, *Catal. Today* **2004**, *93–95*, 575–581.
[8] Y. Wang, D. Yang, S. Li, M. Chen, L. Guo, J. Zhou, *Microporous Mesoporous Mater.* **2018**, *258*, 17–25.
[9] B. O. Adebayo, A. Krishnamurthy, A. A. Rownaghi, F. Rezaei, *Ind. Eng. Chem. Res.* **2020**, *59*, 13762–13772.
[10] S. Sonar, J. Giraudon, S. K. P. Veerapandian, R. Bitar, K. Leus, P. Van Der Voort, J. Lamonier, R. Morent, N. De Geyter, A. Löfberg, *Catalysts* **2020**, *10*, 761–781.
[11] S. Dey, G. Dhal, D. Mohan, R. Prasad, *J. Sci. Adv. Mater. Devices* **2019**, *4*, 47–56.
[12] S. Dey, G. C. Dhal, D. Mohan, R. Prasad, R. N. Gupta, *Appl. Surf. Sci.* **2018**, *441*, 303–316.
[13] S. Dey, G. C. Dhal, *Inorg. Chem. Commun.* **2019**, *110*, 107614–107626.
[14] S. Dey, N. S. Mehta, *Resour. Environ. Sustain.* **2020**, *1*, 100003–100018.

[15] E. C. Njagi, C. H. Chen, H. Genuino, H. Galindo, H. Huang, S. Suib, *Appl. Catal. B* **2010**, *99*, 103–110.
[16] S. Grangeon, A. Fernandez-Martinez, F. Warmont, A. Gloter, N. Marty, A. Poulain, B. Lanson, *Geochem. Trans.* **2015**, *16*, 1–16.
[17] Y. Qin, Y. Wang, J. Li, Z. Qu, *Surf. Interfaces* **2020**, *21*, 100657–100664.
[18] L. H. Tjeng, M. B. J. Meinders, J. van Elp, J. Ghijsen, G. A. Sawatzky, *Phys. Rev. B.* **1990**, *41*, 3190–3199.
[19] A. Payan, N. C. Aghdam, J. Soltan, *J. Environ. Chem. Eng.* **2022**, *10*, 107253–107266.
[20] Q. Ye, J. Zhao, F. Huo, J. Wang, S. Cheng, T. Kang, H. Dai, *Catal. Today* **2011**, *175*, 603–609.
[21] Z. Ye, J. M. Giraudon, N. Nuns, P. Simon, N. De Geyter, R. Morent, J. F. Lamonier, *Appl. Catal. B* **2018**, *223*, 154–166.
[22] A. S. Reddy, C. S. Gopinath, S. Chilukuri, *J. Catal.* **2006**, *243*, 278–291.
[23] V. P. Santos, M. F. R. Pereira, J. J. M. Órfão, J. L. Figueiredo, *Appl. Catal. B* **2009**, *88*, 550–556.
[24] Z. Qu, Y. Bu, Y. Qin, Y. wang, Q. Fiu, *Appl. Catal. B* **2013**, *132*, 353–362.
[25] L. Zhang, S. Zhu, R. Li, W. Deng, C. Hong, D. Liu, L. Guo, *ACS Appl Nano Mater.* **2020**, *3*, 11869–11880.
[26] X. Zhai, F. Jing, L. Li, X. Jiang, J. Zhang, J. Ma, W. Chu, *Fuel* **2021**, *283*, 118888–1188900.
[27] J. Li, Z. Qu, Y. Qin, H. Wang, *Appl. Surf. Sci.* **2016**, *385*, 234–240.
[28] J. Deng, S. He, S. Xie, H. Yang, Y. Liu, G. Guo, H. Dai, *Environ. Sci. Technol.* **2015**, *49*, 11089–11095.
[29] L. Li, Md A. Wahab, H. Li, H. Zhang, J. Deng, X. Zhai, M. Masud, Md S. Hossain, *ACS Appl.Nano Mater.* **2021**, *4*, 6637–6647.
[30] J. Zhu, W. Zhang, Q. Qi, H. Zhang, Y. Zhang, D. Sun, P. Liang, *Sci. Rep.* **2019**, *9*, 12162–12171.
[31] T. Dargel, R. Hertwig, W. Koch, *Mol. Phys.* **1999**, *96*, 583–591.
[32] J. Luo, Q. H. Zhang, J. Garcia-Martinez, S. L. Suib, *J. Am. Chem. Soc.* **2008**, *130*, 3198–3207.
[33] M. Baldi, E. Finocchio, F. Milella, G. Busca, *Appl. Catal. B* **1998**, *16*, 43–51.
[34] C. Cellier, V. Ruaux, C. Lahousse, P. Grange, E. M. Gaigneaux, *Catal. Today* **2006**, *117*, 350–355.

Manuscript received: July 23, 2022
Revised manuscript received: October 17, 2022
Accepted manuscript online: October 24, 2022
Version of record online: November 18, 2022